Acceleration insensitive encapsulated silicon microresonator

C. M. Jha,[a] J. Salvia, S. A. Chandorkar, R. Melamud, E. Kuhl, and T. W. Kenny
Department of Mechanical Engineering and Department of Electrical Engineering, Stanford University, Stanford, California 94305, USA

(Received 21 September 2008; accepted 27 October 2008; published online 10 December 2008)

This paper presents the acceleration sensitivity and the resulting vibration-induced phase noise of an electrostatically coupled encapsulated silicon microresonator. External vibrations can produce phase noise in microresonators by generating time-varying stress in the resonant beams. A spring mounted resonator design that reduces the induced axial stress is presented here. Measurements and simulations show that the acceleration sensitivity and the vibration-induced phase noise of this device can be reduced 1000 times smaller than that of the previously published silicon microresonator and 10 times smaller than the commercially used high end SC (stress compensated)-cut quartz resonator. © *2008 American Institute of Physics*. [DOI: 10.1063/1.3036536]

Micromechanical resonators that are compatible with complementary-metal-oxide-semiconductor (CMOS) processes have shown the potential of being used in precision timing and frequency reference applications.[1–3] However, the frequency of a silicon resonator is dependent on many parameters including external environmental accelerations and vibrations. Many applications require the resonator to operate stably in the face of ambient vibrations (e.g., frequency reference in a car or helicopter). It is therefore desirable for the resonator to have minimum sensitivity to these disturbances. The "acceleration sensitivity" of a resonator is an important figure of merit and has been widely studied for quartz crystal resonators.[4–6]

The acceleration sensitivity $\boldsymbol{\Gamma}$ is defined as[4,7]

$$\frac{\Delta f}{f_0} = \boldsymbol{\Gamma} \cdot \boldsymbol{a} = (\Gamma_x a_x + \Gamma_y a_y + \Gamma_z a_z), \tag{1}$$

where Δf is the change in resonator frequency due to the external acceleration $\boldsymbol{a}$ and f_0 is the frequency with no acceleration (often referred to as the "carrier frequency"). Time-dependent acceleration, i.e., vibration, causes vibration-induced phase noise. The relative strength of vibration-induced phase noise with respect to the carrier frequency f_0 is given by[4,7]

$$\mathcal{L}(f_0 \pm f_v) = 20 \log\left(\frac{f_0 \boldsymbol{\Gamma} \cdot \boldsymbol{a}_0}{2 f_v}\right) \quad [\text{dBc}], \tag{2}$$

where $\boldsymbol{a}_0$ is the peak acceleration at vibration frequency f_v. The principal mechanism that causes the acceleration sensitivity is the axial stress experienced by the resonator beams. To reduce the axial stress in the beams of the resonator, a spring mounted double ended tuning fork (DETF)–type resonator is designed and is compared with our previously published basic single-anchored DETF resonator, as shown in Fig. 1.

The silicon DETF structures are fabricated using a CMOS compatible episeal wafer scale encapsulation[8] process. The "tuning fork vibrational mode" for the single-anchored and spring supported resonators is near 1.3 MHz. The spring supported resonator has a lateral mode consisting of the entire resonator vibrating relative to the spring supports at 45 kHz. The single-anchored resonator has a similar mode consisting of the free mass vibrating relative to the anchor at 145 kHz, where the beams are acting as the spring for this mode. As shown in Fig. 1, the resonator is polarized by the dc bias voltage V_{bias} and electrostatically actuated by providing an ac stimulus to the input electrode. An ac is generated at the output electrode due to the change in capacitance as the resonator beams vibrate. The output electrode is connected to an oscillator circuit to obtain a continuous sinusoidal signal at the frequency f_0. The theoretical model and the oscillation conditions have been reported before.[9]

The dependence of resonator frequency on the axial load P is given by[10]

$$f = \frac{\lambda^2}{2\pi l^2}\left(1 + \frac{P l^2}{EI\pi^2}\right)^{1/2}\left(\frac{EI}{m}\right)^{1/2}, \quad \lambda = 4.73, \tag{3}$$

where λ is a dimensionless parameter that is a function of the boundary conditions applied to the beam and is equal to 4.73

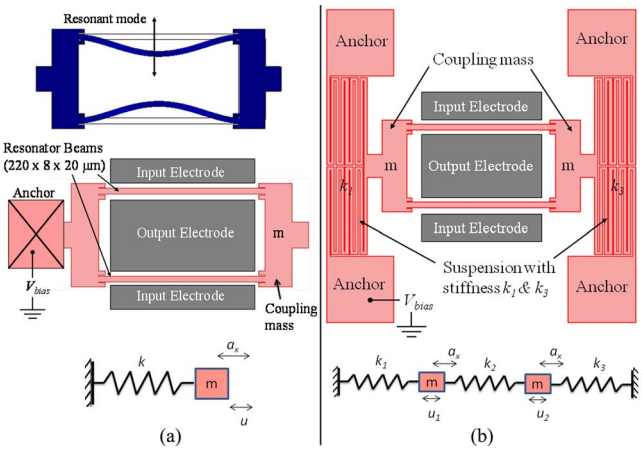

FIG. 1. (Color online) (a) The schematic of a single-anchored DETF resonator with the resonant mode. The effect of the external acceleration a_x is modeled by a spring mass system, where m is the coupling mass, k is the stiffness of the resonator beam, and u is the displacement due to inertia force generated by the external acceleration a_x. (b) The schematic of a spring supported DETF resonator showing serpentine-type resistive silicon suspension on both sides of the resonator with stiffness k_1 and k_3. The stiffness of the resonator beam, in this case, is represented by k_2.

[a]Electronic mail: cmjha75@gmail.com.

for a free-free or clamped-clamped beam, l is the length of the beam, E is the modulus of elasticity, I is the area moment of inertia of the beam about the neutral axis, and m is the mass per unit length of the beam.

The axial load P experienced by the resonator beam can be estimated with the help of a static analysis using a lumped spring mass model, as shown in Fig. 1. The axial load due to external acceleration a_x for the basic DETF structure is given by

$$P_{\text{standard}} = ku = ma_x, \tag{4}$$

where m is the lumped mass (coupling mass+half the mass of the beams) and k is the stiffness of the resonator beam. The mass of the beam is included in the calculation of the lumped mass to account for the effect of the distributed mass of the beam on the axial load. From Eqs. (3) and (4), the change in frequency Δf is estimated to be approximately 0.01 Hz for 1 g of acceleration resulting in the acceleration sensitivity Γ_x of approximately 6.5 ppb/g from Eq. (1).

For the spring supported DETF structure, the axial load is given as

$$P_{\text{spring supported}} = k_2(u_2 - u_1) = ma_x\left(\frac{k_3 - k_1}{k_1 + \frac{k_1 k_3}{k_2} + k_3}\right), \tag{5}$$

where k_2 is the stiffness of the resonator beam and k_1 and k_3 are the stiffnesses of the mechanical suspension on both sides of the resonator. As can be seen from Eq. (5), if k_3 is equal to k_1, i.e., the left and the right support are equally stiff, then the axial load experienced by the resonator beam tends to zero. It should be mentioned that this lumped model is effective only when $k_2 \gg k_3, k_1$, and it can be assumed that the inertia effect of the distributed mass of the resonator beam is negligible. In the case of $k_2 \ll k_3, k_1$, the mass of the resonator beam needs to be accounted for and cannot be neglected. For this design $k_2 \approx 10\,000 k_1$. Since the design of the spring mounted DETF resonator is symmetric [Fig. 1(b)], it can be assumed that $k_1 \approx k_3$, resulting in an acceleration insensitive resonator. However, if we account for the variations in the process parameters of our fabrication process, the difference in k_1 and k_3 can be as high as 5%, resulting in the acceleration sensitivity of up to 0.1 ppb/g. For a simplified theoretical analysis in this paper, we will stick to the assumption of a symmetric design and ignore the error due to fabrication.

The above analysis is based on a simple lumped model and does not capture the effect of the distributed mass of the resonator beams. To investigate this, a finite element simulation (FEM) is performed for both basic and spring mounted structures, assuming the design of the spring supported resonator to be symmetric. We first perform a plane stress static analysis with a body load (force per unit volume) corresponding to the applied external acceleration to find out the resultant stress in the resonator beams. Then, we carry out an eigenfrequency analysis of the same resonant structure under the prestressed condition. The resulting eigenfrequency corresponds to the frequency of the resonator beam under axial stress. Figure 2 shows the plot of change in frequency with respect to the magnitude of the external acceleration. The slope of the curve, which is the acceleration sensitivity Γ_x, is approximately 7.9 ppb/g for the basic DETF resonator. However, for the spring mounted DETF resonator, the acceleration sensitivity is found to be less than 0.01 ppb/g, which is in compliance with the analytical result for the symmetric spring supported design. Further analysis and FEM simulations confirm that there is no first order sensitivity to acceleration in the y and z directions.

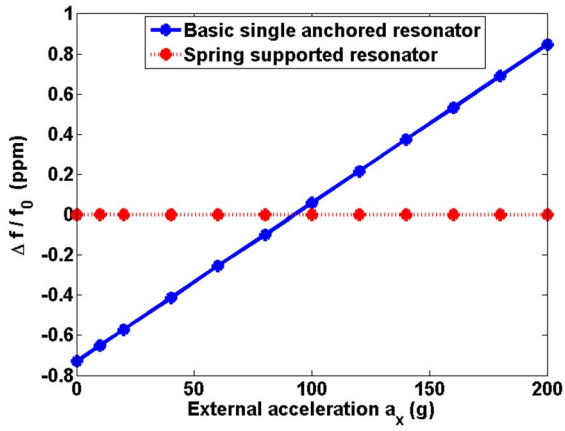

FIG. 2. (Color online) Finite element simulation showing the change in frequency with respect to the acceleration.

For the experimental measurement, a dynamic vibration method was used. One device each from the spring mounted DETF resonator and the basic DETF resonator was tested for collecting experimental data. The device attached on the printed circuit board (PCB) was mounted on a shaker and subjected to a sinusoidal vibration in the x direction at frequencies of 80, 150, and 220 Hz with accelerations ranging from 0 to 30 g. A typical measurement result for 30 g acceleration at 150 Hz is shown in Fig. 3. The amplitude of the acceleration is measured by using a laser vibrometer. The presence of sinusoidal vibration at 150 Hz causes sidebands in the basic single-anchored DETF resonator [Fig. 3(a)] at an offset of 150 Hz from the carrier frequency f_0. However, the sidebands in the spring mounted DETF resonator for the same frequencies and the acceleration range are buried into the noise [Fig. 3(b)]. The relative strength of vibration-induced phase noise (sidebands) with respect to the carrier frequency f_0, $\mathcal{L}(f_0 \pm f_v)$, for the basic DETF resonator is measured to be −57 dBc, which is close to the estimated value of −54 dBc; for the spring mounted DETF resonator, the measured value is less than −85 dBc, whereas the theoretically estimated value is approximately −110 dBc. It should be mentioned that the actual acceleration sensed by the resonator structure might be slightly different from the

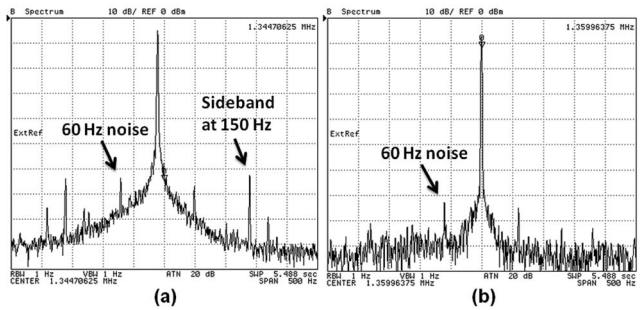

FIG. 3. Experimental result for 150 Hz vibration and 30 g acceleration showing (a) sidebands (−57 dBc) in the spectrum of the basic DETF resonator and (b) no visible sidebands (<−85 dBc) in the spectrum of the spring supported resonator.

measured acceleration due to the damping and vibration associated with the natural frequency of the fixture on which the PCB was mounted. However, the related errors are assumed to be small as the measured result correlates well with the analytical and simulated result [Fig. 3(a)]. Measurements were also done in the y and z directions for up to 30 g and no sidebands were observed. As predicted by the analytical model and the finite element simulations, and also supported by the previous publication,[7] we conclude that there is only a weak sensitivity to acceleration in the y and z directions.

It is to be noted that the above experimental result corresponds to only one spring mounted DETF resonator. However, the experimental data for the multiple basic DETF resonators have been earlier reported,[7] and the theoretical FEM simulation has been shown to be close to the experimental result both in the previous publication[7] as well as in this paper. Similarly, the FEM simulation for the spring mounted DETF resonator correlates well with the experimental data presented above.

One possible disadvantage of this spring mounted DETF resonator could be the increased flexibility of the structure resulting in a substantial change in capacitive gap of the electrostatically actuated resonator and possible damage of the device by snapping the resonator beam into the electrode, under impact. However, this problem can potentially be mitigated in the future by optimizing the design of the resonator structure.

This work was supported by DARPA HERMIT (ONRN66001-03-1-8942), the Robert Bosch Corporation Palo Alto RTC, a CIS Seed Grant, The National Nanofabrication Users Network facilities funded by the National Science Foundation under Award No. ECS-9731294, and the National Science Foundation Instrumentation for Materials Research Program (DMR 9504099). The authors would also like to acknowledge Dr. Matt Hopcroft, Dr. Bongsang Kim, Dr. John Vig, Dr. Yoongkee Kim, Dr. Manu Agarwal, Professor Clark Nguyen, and Professor Amit Lal for their support and inspiration.

[1] C. T.-C. Nguyen, IEEE Trans. Ultrason. Ferroelectr. Freq. Control **54**, 251 (2007).
[2] V. Kaajakari, J. Kiihamaki, A. Oja, S. Pietikainen, V. Kokkala, and H. Kuisma, Sens. Actuators, A **130**, 42 (2006).
[3] C. T.-C. Nguyen and R. T. Howe, IEEE J. Solid-State Circuits **34**, 440 (1999).
[4] R. L. Filler, IEEE Trans. Ultrason. Ferroelectr. Freq. Control **35**, 297 (1988).
[5] R. Beeson, J. J. Gagnepain, D. Janiaud, and M. Valdois, Proceedings of the Frequency Control Symposium, 1979 (unpublished), p. 337.
[6] J. R. Vig, C. Audoin, L. S. Cutler, M. M. Driscoll, E. P. EerNisse, R. L. Filler, R. M. Garvey, W. J. Riley, R. C. Smythe, and R. D. Weglein, Proceedings of the Frequency Control Symposium, 1992 (unpublished), p. 763.
[7] M. Agarwal, K. K. Park, S. A. Chandorkar, R. N. Candler, B. Kim, M. A. Hopcroft, R. Melamud, and T. W. Kenny, Appl. Phys. Lett. **90**, 014103 (2007).
[8] R. N. Candler, M. A. Hopcroft, B. Kim, W.-T. Park, R. Melamud, M. Agarwal, G. Yama, A. Patridge, M. Lutz, and T. W. Kenny, J. Microelectromech. Syst. **15**, 1446 (2006).
[9] Y.-W. Lin, S. Lee, S.-S. Li, Y. Xie, Z. Ren, and C. T.-C. Nguyen, IEEE J. Solid-State Circuits **39**, 2477 (2004).
[10] R. D. Blevins, *Formulas for Natural Frequency and Mode Shape* (Krieger, Malabar, 1984), pp. 101–110 and 143–146.